IEEE Access
Multidisciplinary | Rapid Review | Open Access Journal

SPECIAL SECTION ON EMERGING TRENDS, ISSUES AND CHALLENGES FOR ARRAY SIGNAL PROCESSING AND ITS APPLICATIONS IN SMART CITY

Received December 9, 2019, accepted January 4, 2020, date of publication January 9, 2020, date of current version January 16, 2020.

Digital Object Identifier 10.1109/ACCESS.2020.2965233

RSSI-Based Direction-of-Departure Estimation in Bluetooth Low Energy Using an Array of Frequency-Steered Leaky-Wave Antennas

MIGUEL POVEDA-GARCÍA, ANTONIO GÓMEZ-ALCARAZ, DAVID CAÑETE-REBENAQUE, (Member, IEEE), ALEJANDRO SANTOS MARTINEZ-SALA, AND JOSÉ LUIS GÓMEZ-TORNERO, (Senior Member, IEEE)

Department of Information and Communications Technologies, Technical University of Cartagena (UPCT), 30202 Cartagena, Spain

Corresponding author: Miguel Poveda-García (miguel.poveda@upct.es)

This work was supported in part by the Spanish National projects TEC2016-75934-C4-4-R and TEC2016-76465-C2-1-R, and in part by the 2018 UPCT Santander Research Grant.

ABSTRACT This paper presents a novel advanced Bluetooth Low Energy (BLE) beacon, which is based on an array of frequency-steered leaky-wave antennas (LWAs), as a transmitter for a Direction-of-Departure (DoD) estimation system. The LWA array is completely passive, fabricated in a low-cost FR4 printed-circuit board and designed to multiplex to different angular directions in space each one of the three associated BLE advertising channels that are used for periodically transmitting the ID of the beacon. This way, the use of more expensive hardware associated to electronic phased-array steering/beam-switching is avoided. Four commercial BLE modules are connected to the four ports of the array, producing an advanced BLE beacon that synthesizes twelve directive beams (one per each port and advertising channel) distributed over a wide Field of View (FoV) of 120 degrees in the azimuthal plane. Then, any BLE enabled IoT device located within this FoV can scan the messages from the beacon and obtain the corresponding Received Signal Strength Indicator (RSSI) of these twelve beams to estimate the relative DoD by using amplitude-monopulse signal processing, thus dispensing from complex In-phase/Quadrature (IQ) data acquisition or high computational load. We propose an angular windowing technique to eliminate angular ambiguities and increase the angular resolution, reporting a root mean squared angular error of 3.7° in a wide FoV of 120°.

INDEX TERMS Direction-of-Departure detection, antenna arrays, monopulse systems, leaky-wave antennas, Bluetooth low energy.

I. INTRODUCTION

Bluetooth Low Energy (BLE) is one of the key enabling technologies for the Internet of Things (IoT) revolution in Smart Cities [1]. There are many foreseen scenarios and there is not a single technology to cover all of them, but BLE is probably one of the most promising ones for multiple applications, mainly due to following facts [1]: 1- BLE standard defines a simple and efficient advertising mode to broadcast small messages, called advertisements, and allows a BLE receiver to detect nearby BLE devices. 2- The simplest BLE devices with the advertising feature are called beacons, which are small, cheap, and designed to run on batteries for many months, so they can be easily deployed, with high density, in smart spaces. 3- Off-the-shelf BLE beacons easily interact with commercial smartphones, tablets, or other IoT devices.

This has led to the spread of compelling location service solutions that can be broadly classified on proximity or positioning services [1]. Among the potential uses; proximity, guiding, tracking [2] and localization [3] at indoor scenarios are some of the most important prospective applications.

BLE employs 40 physical narrowband channels in the 2.4GHz ISM band, separated 2MHz between each other. Bluetooth defines two transmission types: data and advertising. Advertising transmission uses three physical radiofrequency (RF) channels (2402 MHz with index #37, 2426 MHz with index #38, and 2480 MHz with index #39) for discovering devices, initiating a connection, and broadcasting data. Data transmission uses up to 37 RF channels for communication between connected devices. As defined in the standard,

The associate editor coordinating the review of this manuscript and approving it for publication was Liangtian Wan.

an advertising message has a header and a payload between 0-31 bytes. It's worth to mention that iBeacon is a proposal from Apple that adopt the BLE standard but specifies its own message format embedded on the payload [1], [3]. The same occurs with the Eddystone format that comes from a Google's proposal. Nowadays, there are the following BLE standards; 4.0, 4.1, 4.2, 5.0 and the recent 5.1 [4], [5]. The basic advertising mechanism, message formats and the scanning process are the same for all the standards, in order to allow compatibility between available commercial products. BLE standards do not specify how to get the advertising channel (#37, #38 or #39) from an incoming message, but it is defined how to indicate the Media Access Control (MAC) address, data payload and the Received Signal Strength Indicator (RSSI) to the application layer.

Current BLE localization services [1] are mainly based on the acquisition of the RSSI from the advertising messages transmitted by a beacon. Three different techniques are used for such RSSI-based location: lateration, fingerprinting and angulation [6]. BLE lateration is based on ranging estimation and, despite being the simplest approach, it provides inaccurate distance estimations due to multipath fading [7], [8]. The BLE fingerprinting approach provides more accurate predictions, but it relies on cumbersome on-site surveys to construct the reference radio map [9], [10]. More recently, angular-based location techniques have been proposed for BLE positioning, showing superior performance than ranging techniques [11], [12], while dispensing from time-consuming fingerprinting radio-maps acquisition.

The new released standard Bluetooth 5.1 [5] pays attention on direction finding capabilities and defines two different methods called Direction-of-Arrival (DoA) and Direction-of- Departure (DoD). Special frame signaling and synchronization for In-phase/Quadrature (IQ) data measurement is required, in addition to high processing power necessary to run the algorithms to identify the direction the Bluetooth signal is coming from. The standard is based on the traditional approach for RF angular estimation [13]. For the DoA architecture, the phased array acts as a scanner, acquires the IQ data and estimates the direction at which a signal has been received from the device with a single antenna that has the role of the BLE beacon. For the case of DoD, the phased array is the BLE beacon and the device with a single antenna has the BLE scanner that receives the IQ data from the phased array and calculates the direction at which the signal has been transmitted with respect to the beacon. Our proposal follows the approach of the second architecture (DoD), since it is more interesting to deploy the beacon in fixed known position, equipped with a phased array and transmitting advertising frames in a predefined sequence. Then, the DoD is estimated from the point of view of a mobile device with a single antenna, such as a smartphone or a tablet, that receives the advertising frames from the phased array and processes them. This way, the computational load is left for the mobile device and the power consumption of the beacon is reduced, extending its lifetime in the case it runs with batteries. It has to be emphasized that the IQ-based direction finding capability is not backward compatible with the previous BLE standards and current BLE Commercial Off-The-Shelf (COTS) products that only provide RSSI information, as it was demonstrated for WiFi [14] and for BLE [15]. For this reason, seeking backward compatibility with BLE standards, we focus on DoD estimation at a mobile device based on RSSI with no IQ data. This RSSI-based angular estimation was demonstrated to show good performance in [16].

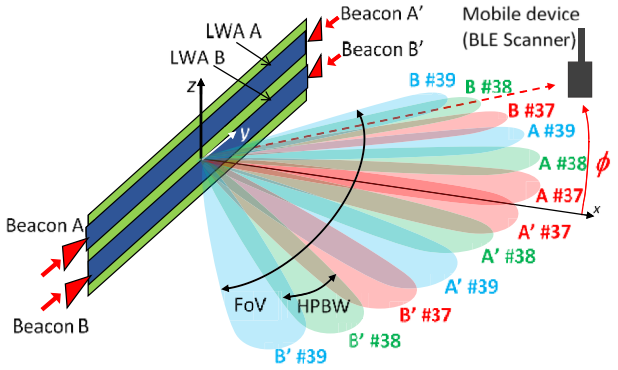

FIGURE 1. Scheme of the advanced BLE beacon with frequency-steering LWA array synthesizing twelve beams using BLE advertising channels #37, #38 and #39 and a mobile device with a BLE scanner.

Due to the lack of IQ data, the estimation of DoD using RSSI information requires a smart antenna at the transmitter that creates multiple partially-overlapped directive beams pointing at different directions of space [16], [17], as shown in Fig. 1. For good resolution, each individual beam must have a narrow Half Power Beam Width (HPBW), while assuring a wide Field of View (FoV) by steering all the beams in a wide angular range. The main types of smart antennas proposed for RSSI-based angular estimation are: switched beam antennas (SBA) [16], [18], electronically steerable parasitic array radiator (ESPAR) antennas [19]–[21], monopulse antennas (MA) [22]–[28], and leaky-wave antennas (LWAs) [29]–[35]. These designs typically implement some type of electronic technique to steer the directive beams over the FoV. This ultimately relies on electronically reconfigurable RF front-end circuits (RF switches, phase shifters, varactors) that increase the cost of the active smart antenna. On the other hand, LWAs show the inherent property of creating frequency-steered directive beams, so that different frequencies are radiated in distinct directions. This has been proposed for Radio Frequency Identification (RFID) location [30], [32], and DoA estimation using wideband RF signals [31] and LWAs. More recently, frequency-steering has been combined with amplitude-monopulse techniques to propose a novel DoA estimation method using an array of two LWAs [35].

In this paper we propose for the first time a totally passive and thus much more efficient and inexpensive smart antenna for BLE RSSI-DoD estimation systems. Its simplicity lies in the use of a frequency-steered LWA in conjunction with the channel-hopping scheme inherent to BLE advertising protocol. We adapt the amplitude monopulse technique proposed

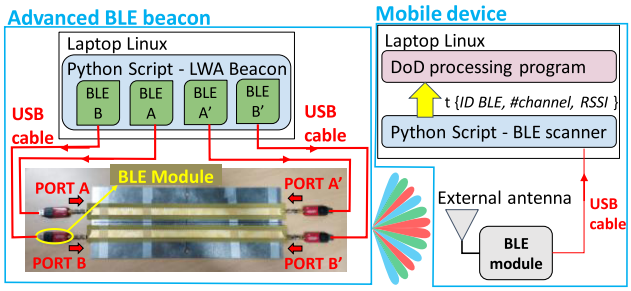

FIGURE 2. Scheme of overall BLE DoD system.

in [35] for the BLE protocol, designing a four-port LWA array whose frequency-steering response matches the three BLE advertising channels. In this way, twelve directive beams angularly distributed in a wide FoV are synthesized when the LWA array is connected to four BLE beacons as sketched in Fig. 1. Therefore, we implement a RSSI-based BLE DoD estimation algorithm that does not require a costly and power-consuming reconfigurable active smart antenna or complex IQ data acquisition, reducing the overall system cost and complexity.

The paper is distributed as follows. Section II describes the advanced BLE beacon with emphasis on the LWA array design. In Section III, the array signal processing to estimate the DoD is explained, demonstrating good angular estimation accuracy in a wide FoV by just measuring the RSSI associated to the twelve directive beams. Finally, Section IV makes a comparison with previous RSSI-based DoA/DoD proposals, to highlight the novelties and benefits of our proposal.

II. ADVANCED BLE BEACON UNIT

A. SYSTEM DESCRIPTION

The scheme of the BLE DoD estimation system is sketched in Fig. 2. The advanced BLE beacon is composed of four BLE modules, acting like beacons and connected to a frequency-steered LWA array with four RF ports (ports A, A', B, B'). A detail of the antenna array is shown in Fig. 3, and it will be described later. In our case, all the BLE modules are controlled by a laptop with Linux, running a script in Python.

The mobile device for this proof of concept is composed of a laptop acting as a control unit and one BLE module configured as a scanner, which is connected to a conventional monopole antenna. The laptop receives the raw data through the BLE module and processes it to estimate the DoD from the advanced BLE beacon. In a real scenario, the receiver can be substituted by a BLE enabled smartphone or tablet with the proper software.

As previously commented, the present BLE standards do not define how to get the advertising channel (#37, #38 or #39) from the incoming message from a beacon, just the MAC address, payload and its RSSI. The channel data at the receiver while complying with the standard is paramount for our proposal. Then we need a beacon that codifies the channel data inside the advertisement message and this information must be easy to retrieve from any consumer or IoT device.

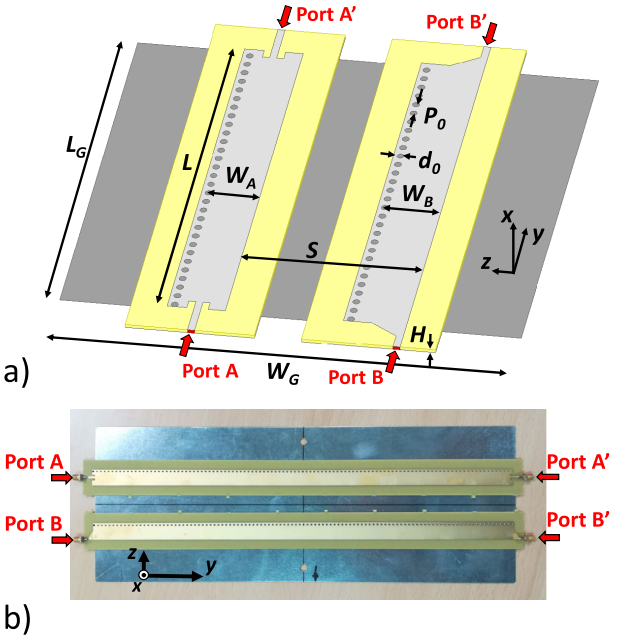

FIGURE 3. a) Scheme and b) picture of designed LWA array.

For this, we employ a similar mechanism as described in [36], following the standard and using the transmission channel map when configuring the beacon transmission. The transmission channel map is a mask that indicates the allowed channels: all of them or just one channel at a time. First, the channel mask is configured for one beacon so it transmits only at channel #37. The MAC address and the payload must be set with a value that easily identifies the BLE module ID and advertising channel being used. Other parameters, such as the interval transmission period between messages (in mseconds) or the total amount of advertising messages can be configured. After the configuration has been performed, the beacon transmits a burst of advertisements in that channel. This process is sequentially repeated for channels #38 and #39. The Python script periodically switches between the four BLE modules so the same sequence is repeated by each one. In our implementation we have used a laptop with Linux, BlueZ library [37], four USB BLE modules [38] and a Python script to command the BLE modules switching periodically on each advertising channel using the iBeacon format. Then, each BLE module acts as a beacon with a known MAC address and transmits 10 messages every 100 msecond, i.e. it stays approximately 1 second per advertising channel. The USB BLE module has a RP-SMA connector and it is bounded to one of the ports of the antenna array. This transmitter (Tx) part is shown on the left side of Fig. 2, and it forms the advanced BLE beacon.

On the other side (right part in Fig. 2), our prototype of mobile device is based on a laptop with Linux, the same USB BLE module [38] connected to a single monopole antenna, a Python script and a DoD estimation processing program. The Python script configures the BLE module as scanner, which periodically reports advertisement events and sends a

TABLE 1. Table with LWA array dimensions in mm according to Fig.3.

Param.	Value	Param.	Value	Param.	Value
L	430	H	1	S	26.6
W_A	14.52	d_0	2	W_G	137
W_B	15.61	P_0	4	L_G	430
G	3.75	S	38	W_G	154

message with raw data (*time stamp, beacon MAC address, #channel, RSSI*) to the DoD processing program. The DoD processing program is a Matlab script that processes the raw data and estimates the DoD.

B. FREQUENCY-STEERED ANTENNA ARRAY

The antenna array is composed of two LWAs arranged in parallel, as shown in Fig. 3. Each LWA provides two opposite input ports to create mirror symmetric beams that are steered with frequency. The half-width microstrip (HWM) LWA technology [39] has been chosen as it was done in [35], due to its simplicity, low-profile planar and compact shape, direct integration with printed-circuit board (PCB) circuits and low-cost characteristics that make it a perfect candidate for IoT applications.

The scheme of the LWA array is depicted in Fig. 3a and the manufactured prototype is shown in Fig. 3b. The array is manufactured using FR4 substrate with thickness $H = 1$ mm, $\varepsilon_r = 4.55$ and $tan\delta = 0.016$. This laminate is widely adopted for low-cost PCB electronics, but it has been recently proposed for its use in LWAs [40] with the aim of reducing the cost of the antenna. Table 1 summarizes the antenna dimensions. Each LWA has a different strip width, W_A and W_B, so to produce complementary frequency-steered responses and achieving a wider FoV for the system as explained in [35]. At one side of each HWM there is a row of metallic vias of diameter d_0 and separated with a period P_0, acting as a perfect electric conductor (PEC) wall; at the other side there is an edge of length L where the radiation occurs. Both antennas are placed with their radiating edges separated at a distance S and on a metallic ground plane with length L_G and width W_G which prevents radiation towards the $-x$ direction and helps increasing the directivity of the LWAs in the space of interest ($+x$ direction).

As it can be observed in Fig. 3a, each of the antennas that compose the array has a different feeding network. For the case of LWA_A, it consists of a microstrip line with an inset in the antenna structure. On the other hand, the feeding network of LWA_B is formed by a microstrip line with a taper (progressive change of the width of the microstrip) and no inset. The reason to use different feeding networks is due to the radiation angular range of each antenna, this is, LWA_A is designed to radiate at angles close to broadside direction ($\phi = 0°$), where the antenna is working close to its cutoff frequency [41], while LWA_B radiates at higher angles. The microstrip line with inset allows for a better matching when working at the lower frequency channel, but as a drawback,

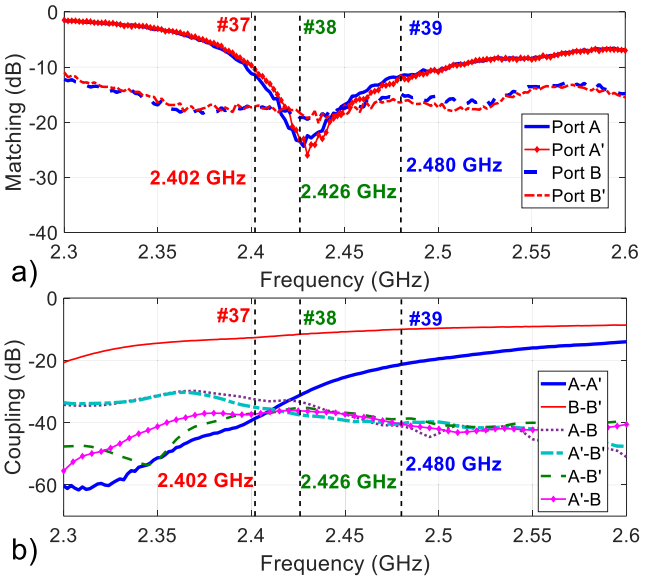

FIGURE 4. Measured LWA array a) Matching. b) Coupling between ports.

the behavior of this feeding network is more resonant, which means that its functional bandwidth is reduced, as it can be observed in Fig. 4a. On the contrary, the microstrip line with taper permits a good matching in a greater bandwidth, but it does no work properly close to the cutoff, which in the case of LWA_B is far below the BLE advertising channels. In any case, good matching below -10 dB in the band of interest (2.402-2.48 GHz), is achieved in the four ports of the antenna array as shown Fig. 4a.

It is also important to realize that part of the power that is injected through one port can couple to other ports. This is depicted in Fig. 4b. First, in LWAs, part of the power reaches the end of the structure without being radiated. This amount of power is coupled in the opposite port, as it is represented in the curves A-A' and B-B'. As it can be observed, this coupling increases with the frequency, since the radiation rate is reduced for higher angles [41]. A maximum value of -10 dB is obtained for the case of LWA_B and channel #39. The rest of the couplings are related with the radiated fields that are absorbed by the other ports of the structure. The couplings A-B and A'-B' are between parallel ports, while A-B' and A'-B are the ones relating opposite crossed ports. As can be seen in Fig. 4, all of these couplings are below -30 dB in the whole bandwidth. This shows a good isolation between all the ports of the structure.

The radiation patterns produced by the LWA array in the corresponding BLE channels have been measured in an anechoic chamber as shown in Fig. 5, using a directive panel antenna as a reference. As sketched in Fig. 1, we need the array to generate twelve directive beams pointing at different directions, each beam associated to a single BLE module and a single BLE advertising channel. The radiation patterns have been measured both in the analog domain (using vector network analyzer R&S ZVL6, Fig. 6b) and also in the digital domain (Fig. 6c), i.e., measuring the RSSI levels at

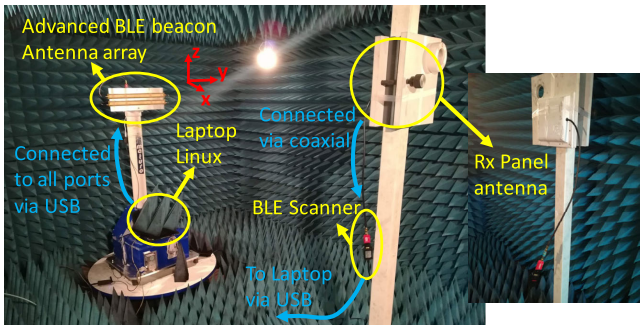

FIGURE 5. Characterization of radiation patterns in anechoic chamber.

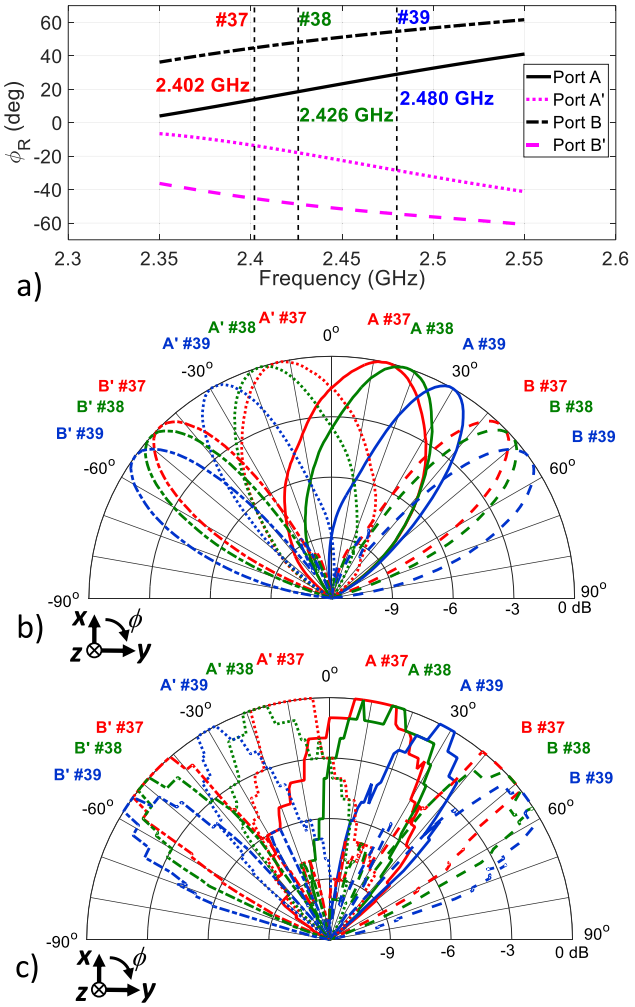

FIGURE 6. Measured frequency-steered array response a) Steering angle ϕ_R b) Analog radiation patterns c) BLE digital radiation patterns.

each angular direction and for the different ports and BLE channels. The measured radiation angle ϕ_R as frequency is varied for each port of the LWA array is shown Fig. 6a. Port A creates the steering angles $\phi_{A\#37}$ =13.7°, $\phi_{A\#38}$ =18.5° and $\phi_{A\#39}$ =29°, while port B produces $\phi_{B\#37}$ =44.5°, $\phi_{B\#38}$ =48° and $\phi_{B\#39}$ =54.5°.Port A' and B' produce beams at mirrored directions (negative values of ϕ).

TABLE 2. Relative peak gain (*RPG*) between channels in dBs.

Port	A			B		
BLE Channel	#37	#38	#39	#37	#38	#39
RPG (analog)	-2	-0.5	0	-0.1	0	-2
RPG (BLE RSSI)	-11	-4	-2	-8	-5	-3.5
Port	**A'**			**B'**		
BLE Channel	#37	#38	#39	#37	#38	#39
RPG (analog)	-2.5	-0.8	-0.4	-0.3	-0.2	-2.2
RPG (BLE RSSI)	-8	-3	0	-7	-3	-2

As it can be seen in Fig. 6c, the digital BLE patterns show quantization in 1 dB steps. This is due to the fact that the BLE receiver [38] produces such quantization in the acquired RSSI levels. In any case, it can be seen how a wide FoV is covered using twelve directive beams.

With these overlapped beams, the DoD can be estimated using different techniques, such as MUSIC (Multiple Signal Classification) [42] or ESPRIT (Estimation of Signal Parameters via Rotation Invariance Techniques) [43]. We propose, as explained in section II.C, the use of amplitude-monopulse processing like it was done in [35], which is robust against changes in the propagation channel.

C. STEERED MONOPULSE FUNCTIONS

The amplitude monopulse technique has been normally applied for DoA estimation, by comparing the relative power levels received by two partially overlapped directive beams [26], [35]. This technique can be reciprocally applied for DoD estimation, measuring the power of a signal received in a mobile device and transmitted from the two overlapped beams. In order to compensate the peak gain difference between different beams and equalize it, a factor must be applied to each beam to normalize the values to the maximum. This calibration has been already done in other works that make use of LWAs for DoA estimation systems [31], [35], [44], but it is also valid for DoD estimation. Table 2 summarizes the peak gain difference or Relative Peak Gain (*RPG*) between channels. For each beam, the peak gain has been compared to the highest value, which in the case of the analog patterns it is achieved using port A with the channel #39 and in the digital patterns it is obtained with port A' using also channel #39.

It can also be observed that the peak differences are much higher in the digital patterns than in the analog ones. This is because the electronics of each BLE module, which can have different performance, are taken into account for the digital patterns. Once the *RPG* between channels and ports has been characterized, the digital monopulse functions MF can be defined from the combination of the sum (Σ) and difference (Δ) of the normalized gain pattern $\bar{G}$ of any pair of

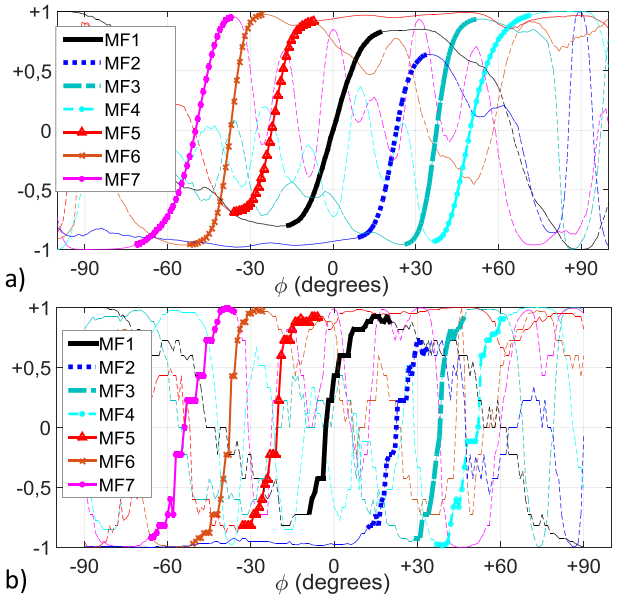

FIGURE 7. Measured monopulse functions a) Analog b) Digital RSSI.

beams as:

$$MF\left(\phi, P_iCh_k, P_jCh_l\right) = \frac{\Delta\left(\phi, P_iCh_k, P_jCh_l\right)}{\sum\left(\phi, P_iCh_k, P_jCh_l\right)} = \frac{\overline{G}\left(\phi, P_iCh_k\right) - \overline{G}\left(\phi, P_jCh_l\right)}{\overline{G}\left(\phi, P_iCh_k\right) + \overline{G}\left(\phi, P_jCh_l\right)} \quad (1)$$

where $\bar{G}(\phi, P_iCh_k)$ indicates the normalized gain pattern (in linear units) using any port P_i (i, j = A, B, A', B') and any channel Ch_k (k, l = 37, 38 or 39), which is obtained as follows:

$$\overline{G}\left(\phi, P_iCh_k\right) = 10^{\left(\frac{G(\phi)|_{dB} - RPG(P_iCh_k)|_{dB}}{10}\right)} \quad (2)$$

It must be highlighted that, in contrast to conventional monopulse systems [35], it is not necessary to use beams at the same frequency. In our case, since the data is processed in the digital domain instead of in the analog RF domain, any pair of beams created at different angles and any frequencies can be compared to estimate the DoD within their partial FoV, leading to *virtual* digital monopulse synthesis. Table 3 summarizes the combination of ports and BLE channels used to generate M = 7 monopulse functions using (1). The monopulse functions are shown in Fig. 7. Apart from the aforementioned digital quantization due to discrete RSSI levels, the obtained digital monopulse functions shown in Fig. 7b are in good agreement with the analog ones in Fig. 7a.

It can be seen that each monopulse function is steered to a different angular region and has its own partial FoV (summarized in Table 3), which complements with the other functions to cover a wide total FoV of [−60°, +60°]. The value obtained in (1) for each MF∈[−1, 1] can be related to a DoD (ϕ value on the abscissa axis) due to its almost linear

TABLE 3. Combination of channels and ports to obtain steered monopulse functions.

MF#	Combination of port and BLE channel	partial FoV	Sensitivity ($dM/d\phi$)
MF1	A#37 & A'#37	[- 11º , +11º]	0.79 (1/10º)
MF2	A#37 & A#39	[+11º , +30º]	1.02
MF3	A#39 & B#37	[+29º , +42º]	1.39
MF4	B#37 & B#39	[+40º , +60º]	1.02
MF5	A'#37 & A'#39	[- 30º , - 11º]	1.09
MF6	A'#39 & B'#37	[- 42º , - 29º]	1.48
MF7	B'#37 & B'#39	[- 60º , - 40º]	0.95

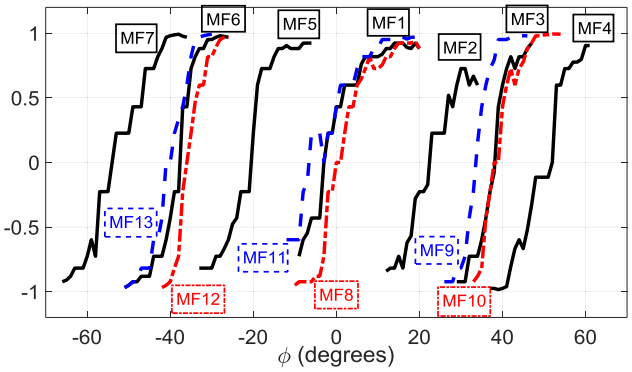

FIGURE 8. Addition of overlapping monopulse functions to mitigate multipath effects.

relation in the partial FoV indicated in Table 3. As the DoD is not known a priori, ambiguity is present in the estimation and signal processing is required, as it will be explained in section III. It is also important to remark that the angular resolution of the system is related to the monopulse sensitivity, which can be measured from the slope of the synthesized monopulse functions (dM/dϕ). High angular resolution is achieved thanks to the narrow beams (so that steep monopulse functions are obtained), but this creates narrow individual FoV too. Here the superposition of all partial FoV creates a wide total FoV, while keeping high angular sensitivity for all monopulse functions, as shown in Table 3. It can be observed that the channel #38 is not used to create any of this monopulse functions necessary to cover the wide FoV, but it can be used to generate six new overlapping monopulse functions that increase the accuracy in case of multipath, as it will be demonstrated later. As shown in Fig. 8, a total amount of M=13 monopulse functions can be synthesized when using all the BLE channels. Their respective combination of beams, local FoV and angular sensitivity are summarized in Table 4.

III. RSSI-BASED DoD ESTIMATION USING STEERED MONOPULSE SIGNAL PROCESSING

The digital monopulse functions characterized in Fig. 8 are the references for the estimation of the DoD with respect to the advanced BLE beacon, as they are measured in a controlled environment with no multipath. Then, in a real scenario, the beacon will work as explained in Section II,

TABLE 4. Combination of channels and ports to obtain overlapping monopulse functions.

MF#	Combination of port and BLE channel	partial FoV	Sensitivity ($dM/d\phi$)
MF8	A#38 & A'#37	[- 8º , +14º]	0.73 (1/10º)
MF9	A#38 & B#37	[+27º , +40º]	1.32
MF10	A#39 & B#38	[+34º , +45º]	1.48
MF11	A'#38 & B#37	[-14º , +8º]	0.72
MF12	A'#38 & B'#37	[- 40º , - 29º]	1.53
MF13	A'#39 & B'#38	[- 45º , - 34º]	1.55

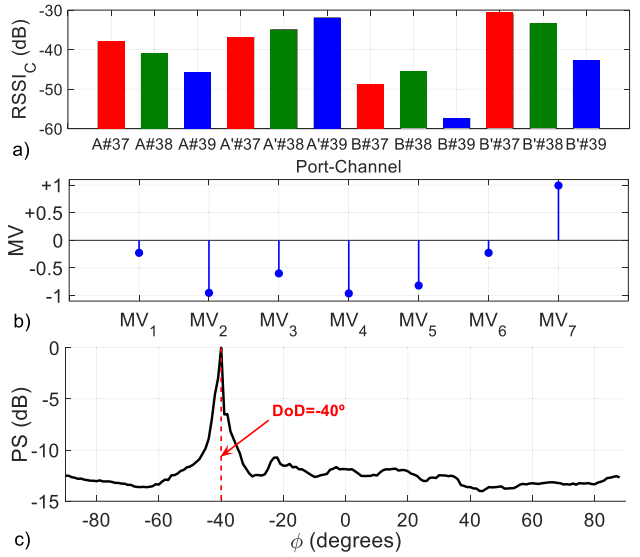

FIGURE 9. Array signal processing.

transmitting BLE advertising messages, sequentially changing the transmission channel and the transmitting BLE module. Once the receiver has gathered information from all channels and ports (vector of twelve elements {RSSI, beam ID}), the DoD estimation will be performed by comparison with the monopulse functions obtained in the anechoic chamber. The processing is quite similar to the analog one presented in [35], but it must be noticed that here we can combine digital information from all channels and ports. This allows to have more virtual monopulse functions for a better performance of the DoD system.

To better illustrate the steps of the signal processing, Fig. 9 shows the results for a particular case in which the real DoD is $\phi = -40°$. First, the BLE receiver acquires the twelve values of RSSI corresponding to each one of the beams transmitted by the advanced BLE beacon. These RSSI values in dBm must be corrected by the *RPG* in Table 2, so we obtain a calibrated RSSI in dB:

$$RSSI_C\,(P_iCh_k) = RSSI\,(P_iCh_k) - RPG\,(P_iCh_k) \qquad (3)$$

where i indicates the port (A, A', B, B') and k indicates the channel (#37, #38, #39). The value of the $RSSI_C$ for each channel and port is represented in Fig. 9a, having a total of 12 values, one for each beam in Fig. 6c. After this, a monopulse value MV_m can be obtained from the

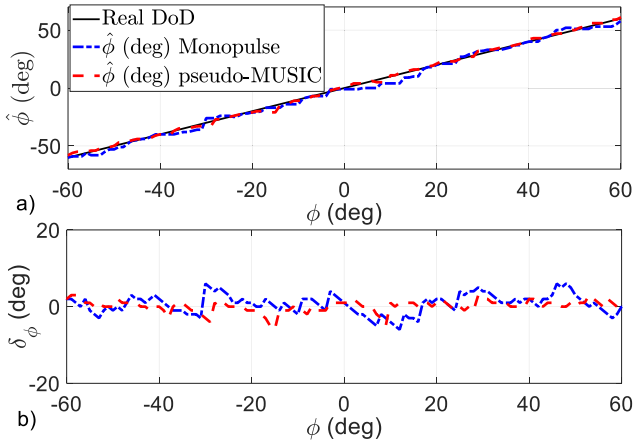

FIGURE 10. a) Estimated DoD ($\hat{\phi}$) and b) estimation error (δ_ϕ) in anechoic chamber. Monopulse and pseudo-MUSIC processing are compared.

combination of any pair of $RSSI_C$ values:

$$MV_m = \frac{10^{RSSI_C\,(P_iCh_k)/10} - 10^{RSSI_C\,(P_jCh_l)/10}}{10^{RSSI_C\,(P_iCh_k)/10} + 10^{RSSI_C\,(P_jCh_l)/10}} \qquad (4)$$

where the index m = 1..7 corresponds to the combination of ports and BLE channels, with the same order as presented in Table 3. Thus, we obtain seven monopulse values that are depicted in Fig. 9b. After this, each monopulse value is compared to its correspondent monopulse function (Fig. 7b), obtaining an individual monopulse error function *ME* which depends on the unknown angular direction ϕ as follows:

$$ME_m\,(\phi) = abs\,(MF_m\,(\phi) - MV_m) \qquad (5)$$

Then, in order to take into account all monopulse functions and eliminate ambiguities, we define a pseudospectrum $PS(\phi)$ as the normalized inverse of the root mean square error (RMSE) of all monopulse errors for each angle:

$$PS_M\,(\phi) = -10\log\left(\left(\frac{1}{\sqrt{\sum_{m=1}^{M}\frac{1}{M}ME_m\,(\phi)^2}}\right)\right) \qquad (6)$$

The estimated DoD ($\hat{\phi}$) will be the angle ϕ where the PS shows a maximum value (minimum RMSE). This is represented, in Fig. 9c, where it can be seen that there is a maximum at $\phi = -40°$, showing an agreement with the real DoD in the measurement. The example in Fig. 9 was performed inside the anechoic chamber shown in Fig. 5 at a distance of 3 m between the advanced BLE beacon and the BLE scanner. Similarly, the DoD has been estimated in the entire FoV of 120°, in steps of 1° as plotted in Fig. 10.

Fig. 10a shows the estimated DoD while the estimation error is plotted in Fig. 10b. As it can be seen, the DoD is estimated in the entire FoV of 120°, with a maximum error of 6° and a RMSE of only 2.6°. In addition, it can be seen

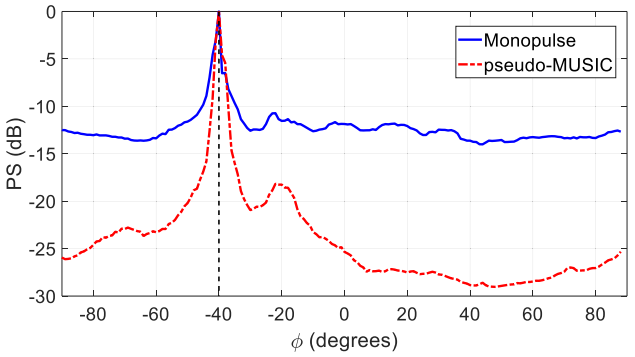

FIGURE 11. Comparison between monopulse and pseudo-MUSIC angular pseudospectrums for a DoD of 40° in anechoic chamber.

that the angular estimation error is independent on the angle. Normally, reconfigurable systems have poorer performance when working far from the normal direction ($\phi = 0°$), due to the lower beam directivity when approaching to endfire ($\phi = \pm 90°$). In our frequency-steerable LWA array this is not the case; as it is shown in Fig. 6, the beams are more directive for higher pointing angles than for the normal direction. As explained in [35], the leaky-wave antenna produces a broader beam at broadside due to the higher losses suffered by the travelling wave under these radiation conditions. Consequently, the monopulse function sensitivity is almost constant for all directions, as summarized in Table 3, and the angular estimation performance does not depend on the steered direction.

At this point, it is important to highlight that other angular estimation algorithms such as MUSIC or ESPRIT could have been adapted to estimate the DoD with the LWA array. These methods use angular steering vectors to define the signal subspace. A power-based adaptation of the MUSIC algorithm was applied for electronically reconfigurable LWAs in [34], without the need of phase information of the signals, and this can similarly be adapted for a frequency-steered LWA as the one used here. In our case, once the RSSI values have been acquired and stored for the twelve directive beams as shown in Fig. 9a, they define a power input vector for the unknown DoD. This vector can be compared to the premeasured power steering vectors for different angular directions to plot an angular or spatial pseudo-MUSIC spectrum and eventually estimate the angular direction from its peaks. In Fig. 11, the pseudo-MUSIC angular spectrum for the example in Fig. 9 is compared to the PS obtained from the steered monopulse functions as defined in (6). As it can be seen, both angular spectrums show similar shape and present a peak in the correct value of the DoD. Besides, the DoD estimated with pseudo-MUSIC is compared to our approach in Fig. 10, showing similar performance in the anechoic chamber. It must be remarked that both the pseudo-MUSIC and the steered monopulse signal processing technique are compatible DoD estimation algorithms for smart multi beam antennas. As commented, an adapted MUSIC algorithm has been applied to estimate angle with electronically-steerable LWAs [29], [33], [34] and with switched steered monopulse

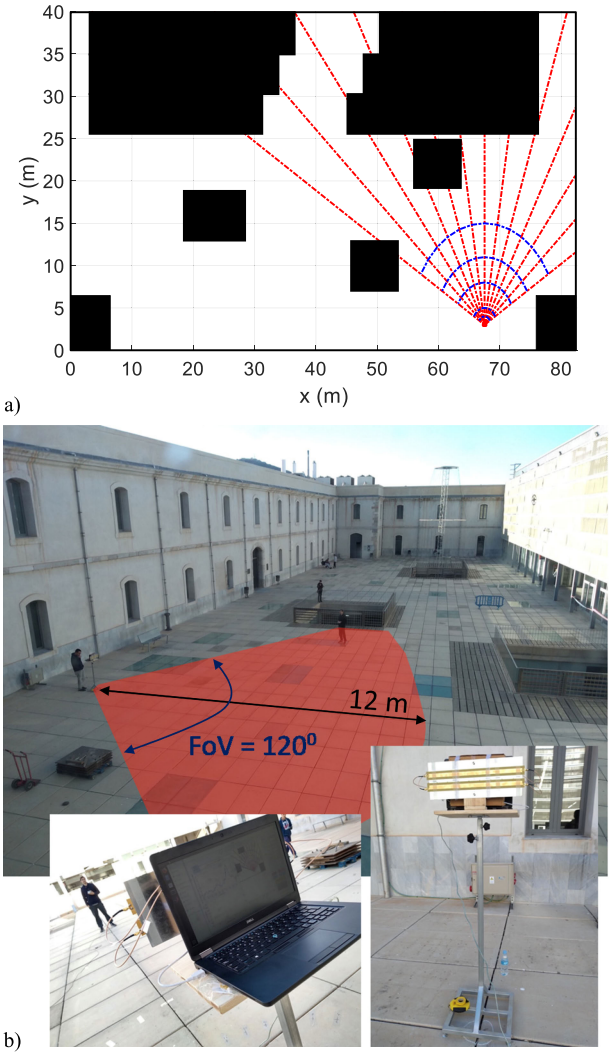

FIGURE 12. Outdoor scenario at UPCT campus a) Layout b) Picture.

antennas [27], [28]. The main contribution of our proposal is the technique to create the multiple steered beams that provide the angular information. While previous smart antennas need electronic reconfiguration to steer the beam and produce the steering vectors, our proposal uses a frequency-steering technique which perfectly suits with the inherent channel-hopping advertising scheme of BLE to avoid any active, power consuming electronic reconfiguration of the antenna beam direction. Certainly, our proposal is smarter in the sense that a passive smart antenna produces even better performance than active beamforming BLE beacons, as it will be explained in a detailed comparison in section IV.

Next test is performed in an outdoor scenario with possible multipath. The scheme of the measurement grid is depicted in Fig. 12a, showing the location of different obstacles and walls with respect to the transmitter and showing the measurements zone. To cover the whole FoV, the test points were located from $\phi = -60°$ to $\phi = +60°$ in 10° steps. Also, to test the robustness of the system with respect to variations in the distance between the BLE advanced beacon and the

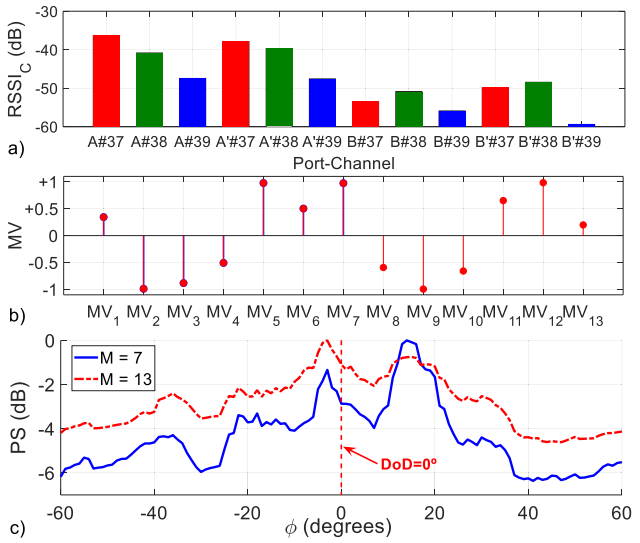

FIGURE 13. Effect of using more monopulse functions to reduce multipath effects.

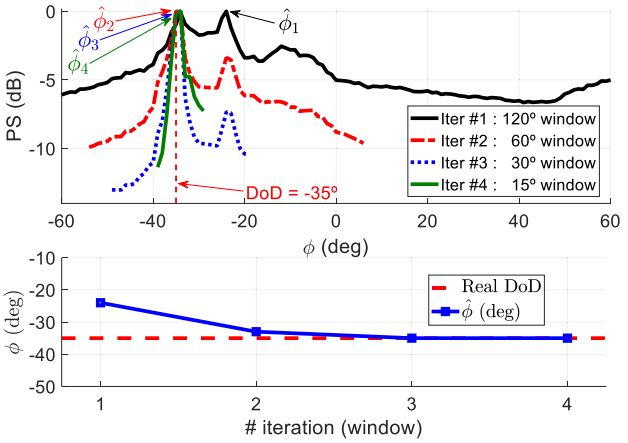

FIGURE 14. Iterative spatial windowing to reduce noise and multipath effects.

mobile IoT device, the measurements were also performed for different radial distances: 1, 2, 5, 8 and 12 m. A total of 65 points were measured in this grid. As shown in Fig. 12b, the advanced BLE beacon is mounted on a tripod at a height of 1.5 m, and the IoT device has a dipole antenna with vertical orientation and it is carried by a person.

In the presence of multipath, the use of as much monopulse functions as possible is beneficial for the DoD estimation. To demonstrate this, Fig. 13 shows the results for the case of a real DoD of $\phi = 0°$, at a distance of 8 m, using a total of M = 7 (from MF1 to MF7) and M = 13 (from MF1 to MF13) monopulse functions. First, as it was done in the test in anechoic chamber, we represent the $RSSI_C$ for all the channels and ports. Again, we have a total of 12 values, shown in

Fig. 13a. Now, as depicted in Fig. 13b, we can obtain more monopulse values using (4), corresponding to each of the additional monopulse functions (MF = 8 ... 13). Thus, when obtaining the pseudospectrum $PS(\phi)$, we will use more error functions. In Fig. 13c, the $PS(\phi)$ is represented when using M = 7 and M = 13 monopulse values. Using M = 7 monopulse functions, it can be observed that there are two peaks in the pseudospectrum. Apart from the peak around $\phi = 0°$ due to the real DoD, another maximum appears around the angle $\phi = +15°$ due to multipath effects. If M = 7 monopulse functions are used, the dominant contribution is the one of the multipath, leading to a wrong DoD estimation. However, using M = 13 monopulse functions the multipath influence is mitigated. The two peaks are still present, since the multipath effect is not eliminated, but now the dominant contribution in the PS leads to a lower DoD estimation error.

As a drawback, it must be remarked that the use of more monopulse functions increases the bias level observed in the PS in Fig. 13b (from a floor level of −6 dB with M = 7 to −4 dB with M = 13). This reduces the dynamic range for DoD estimation. In order to reduce the error coming from this noise and also to help mitigating the multipath effect, it would be convenient for a good estimation to use only the monopulse functions with their partial FoV containing the real DoD, but this cannot be known a priori. For this, an iterative spatial windowing is applied as illustrated in Fig. 14 for a case with real DoD $\phi = -35°$. In the first iteration, an initial estimation of the DoD is performed using all the M = 13 monopulse functions in the total 120° FoV [−60°, +60°].

This first estimation is defined as $\hat{\phi}_1$ and for the example in Fig. 14 led to $\hat{\phi}_1 = -24°$. Then, a second iteration is performed, but now using just the monopulse functions whose partial FoV falls on a window of half the angular range of the previous iteration #1 (60°) and centered on $\hat{\phi}_1$. For the example shown in Fig. 14, a total of M = 8 monopulse functions were used in this second step, corresponding to those falling in Fig. 8 within the angular interval $\phi = [-54°, +6°]$. This provides the second estimation $\hat{\phi}_2 == -32°$. The iterations continue until two consecutive iterations result in the same estimated angle, which in our example occurs in the fourth iteration ($\hat{\phi}_3 = \hat{\phi}_4 = -35°$). Two issues must be noticed in the results of Fig. 14. First, the peak due to the multipath, which in the first iteration leads to a wrong estimation, is reduced in every iteration. Second, the noise floor level in the pseudospectrum drops with each iteration (from −5dB to −10dB), as a consequence of reducing the amount of monopulse functions used. As it can be seen, the peaks in the PS become sharper with each iteration, therefore improving the angular resolution and accuracy. Finally, the iterative windowing process converges to a more accurate DoD estimation.

One last test is performed in order to analyze the robustness of the system when the orientation of the mobile device is changed or when there are obstacles between the device and the advanced BLE beacon. For this, first we estimate the DoD when the mobile device is facing the beacon at the same height. In Fig. 15a the values of received RSSI for one of the ports and the three BLE channels, are plotted.

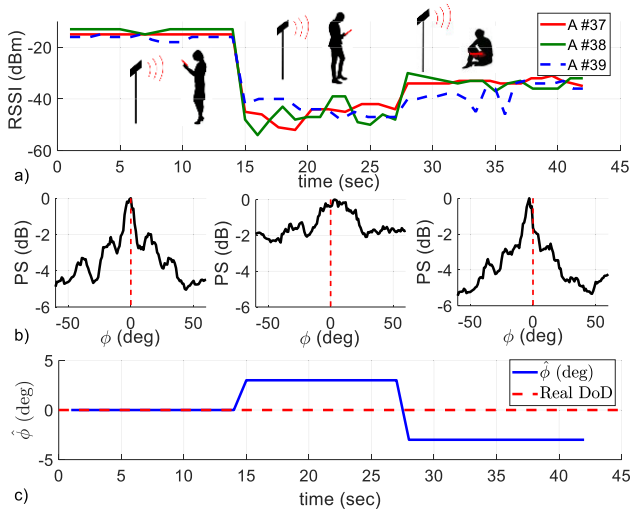

FIGURE 15. Robustness with respect to mobile orientation.

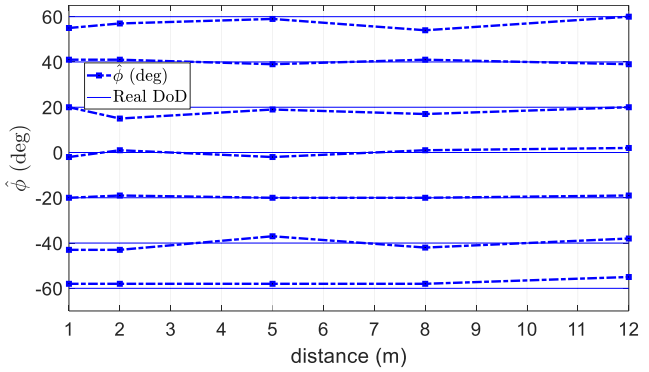

FIGURE 16. Estimation of DoD as a function of distance.

For the first 15 seconds, the device keeps in the same position with nothing blocking the direct line of sight. The PS shown in Fig. 15b for this case is very clean and the system predicts perfectly the real DoD, as shown in Fig. 15c. The second case of study is with the person holding the mobile device backwards to the beacon, thus blocking the line of sight with their body. Now it can be noticed in Fig. 15a that the RSSI levels are much lower than in the previous case, due to the attenuation created by the body in between.

Also, the pseudospectrum for this case shown in Fig. 15b is noisier and shows a higher background noise level due to the lower acquired RSSI levels. Nevertheless, the estimation of the DoD is quite good, with an error of 3°. At this point it must be remarked that monopulse systems are known to provide range-free angular estimation, i.e., they are robust with respect to absolute power variations [26], since the DoD estimation is based on the relative levels acquired by each of the two beams forming the monopulse. This also applies for our monopulse system with twelve beams, which shows robustness when an obstacle reduces the RSSI levels in a similar extent for all the channels, as shown in the 30 dB signal drop of Fig. 15a.

Finally, the device is placed on the floor. The RSSI levels are also lower than in the first case. This is because the gain of the antenna does not keep constant in the elevation xz-plane. As it was explained in [35], this does not affect the DoD estimation as long as we stay in a given angular range, depending on the beamwidth of the radiation patterns in this plane. As can be seen in Fig. 15b, the pseudospectrum is also very clean, and the final estimated DoD has an error of 3° despite the change of height.

In Fig. 16, it is shown the estimated DoD for some of the test points in the grid presented in Fig. 12a (covering five radial distances of 1 m, 2 m, 5 m, 8 m and 12 m, and 13 angular sectors from $\phi = -60°$ to $\phi = +60°$ in 20° steps). In Fig.16, solid lines correspond to the real angles and dashed lines to the estimated DoD. Each solid line, along with its corresponding dashed line represents angular directions $\phi = 0°, \pm 20°, \pm 40°, \pm 60°$. As previously explained, here we can see the robustness of the system with the distance. The absolute variations in the received RSSI are the same for all the ports and channels, so that the relative value between them does not change. As a consequence, we can see that the DoD estimation performance is similar in all the test points, despite the RSSI variations in this range of 12 meters, which obviously define different values of SNR (Signal-to-Noise Ratio).

In order to evaluate the SNR in the experiments, we can compare the background noise level with the maximum and the minimum values of all the received RSSIs. First, the noise power is defined by the well-known expression:

$$N = kT_aB \tag{7}$$

Being $k = 1.38{\cdot}10^{-23}$ J/K, T_a the antenna temperature, which is typically 60K at 2.45 GHz [45], and B is the received signal bandwidth that for the case of the channels of the BLE protocol is 2 MHz. Thus, the noise power is $N = -107.8$ dBm.

In the experiments, the maximum measured RSSI value was $\text{RSSI}_{\text{max}} = -3$ dBm, obtained at a close distance of 1m and at an angle of $\phi = -30°$ with respect to the transmitter. This angle with maximum RSSI value is in accordance with the beam patterns shown in Fig. 6c and the RPG in Table 2: effectively, the beam obtained at channel #39 and port A is the one with the highest peak gain and it is pointing towards this direction $\phi = -30°$. As a result, the maximum SNR value in the experiments was $\text{SNR}_{\text{max}} = 104.8$ dB. On the other hand, a minimum RSSI value of -69 dBm is experimentally obtained at the largest distance of 12 m and for port A and channel #38, leading to a minimum SNR of 38.8 dB. From these results, we can conclude that the SNR in our experiments (covering a distance of 12 meters and a Field of View of 120°) varies in this range between SNR = 105 dB and SNR = 39 dB. Moreover, the sensibility of the receiver BLE module according to the datasheet [38] is -88 dBm, so the measured RSSI values in all the experiments are quite above this value. In any case, the variability in the DoD estimation for the different test locations can be related with the noise in the electronics of the BLE modules and more importantly, due

TABLE 5. Angular error statistics from the experimental test in Fig. 16.

Method	MAE (deg)	RMSE (deg)	50 per. error	90 per. error
M=7 no windowing	6.5	16.2	2.3º	13.5º
M=7 with windowing	5.1	15.5	1.8º	7.8º
M=13 no windowing	4.2	5.9	2.1º	7.8º
M=13 with windowing	2.7	3.7	1.5º	5.8º
Pseudo-MUSIC	3.7	4.9	2.4º	6.7º
Results in [28]	unkown	unkown	3.9º	8.9º

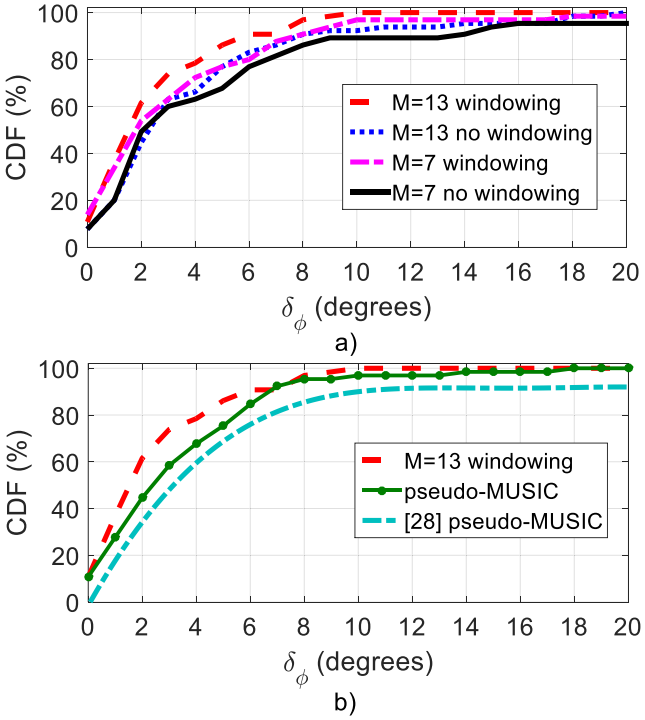

FIGURE 17. CDF of angular error a) Comparison using different number of monopulse functions and windowing technique. b) Comparison with pseudo-MUSIC from our dataset and from results in [28].

to multipath effects which can be reduced with the described signal processing.

For each test point, the angular error, defined as the difference between the real and the estimated angle, is calculated. Also, the Mean Absolute Error (MAE) and the Root Mean Squared Error (RMSE) for the angular error are computed for the 65 test points in the experiment of Fig. 16. The use of M = 7 and M = 13 monopulse functions, with and without the angular windowing technique are compared in Table 5. The MAE is reduced when using more monopulse functions and the windowing technique, from 6.5° (M = 7 and no windowing) to an absolute error of 2.7° for the best case (M = 13 and windowing). The RMSE follows a similar tendency, reporting for the best case a RMSE of 3.7°. Clearly, the use of M = 13 monopulse functions and angular windowing outperforms the other alternatives.

The closer experimental setup to ours is found in [28] with 4 BLE beacons placed on the corners of a room. Each beacon is based on a phased-array antenna with 1 BLE module and switches to steer the beam. The receiver uses a monopole antenna in a tripod and it is conducted a measurement campaign in 65 points around the room with Line-of-Sight (LoS) conditions. The authors calculate the empirical Cumulative Distribution Function (CDF) of the angular error taking into account the real angle and the estimated angle for all the beacons (see Fig.19 in [28]) and the percentile errors. In order to compare with their results, we plot in Fig. 17a the calculated empirical CDF from our field test for different estimation methods. Again, it is shown from the CDF curves the improvement in the performance when using more monopulse functions (M=13) and the windowing technique. For this best case, we achieve a 50 and 90 percentile error of 1.5° and 5.8° respectively. Also, the CDF results from [28] are plotted in Fig.17 for comparison, showing a larger 50 and 90 percentile error of 3.9° and 8.9° respectively as summarized also in Table 5. In [28], a pseudo-MUSIC algorithm was used to estimate the DoD. As previously explained, the better performance of our proposal is not due to the use of monopulse DoD estimation algorithm rather than adapted MUSIC, but to the fact that we synthesize twelve directive steered beams rather than four as in [28]. Besides, the reported FoV in [28] is 80°. Our smart array for BLE DoD finding solution provides wider FoV of 120° and higher angular accuracy. In addition, our smart BLE beacon provides better performance, while being a completely passive antenna and thus dispensing from active beam steering. For instance, the active beamforming smart BLE beacons for DoD estimation proposed in [28] makes use of an active microwave Single Pole 4 Through (SP4T) switch with associated Micro-Controller Unit (MCU) and Beam-Forming Network (BFN) to create four directive switched beams. Clearly, the frequency-steering solution proposed in our work takes advantage of the channel hopping scheduling, inherent to BLE advertising protocol, to avoid any active beam steering method and reduce the smart antenna cost and control complexity, thus being in this sense more efficient and smarter BLE beacon solution than the active phased array used in [28]. Finally, the CDF obtained when applying the pseudo-MUSIC algorithm to our frequency-steered array is also plotted in Fig.17b as a benchmark. The pseudo-MUSIC algorithm produces poorer DoD estimation than our technique with M = 13 monopulse functions and using windowing, as summarized in Table 5. In any case, both DoD estimation algorithms (monopulse and pseudo-MUSIC) show lower angular estimation error than [28] thanks to the use of the frequency-steered antenna which synthesizes a total of 12 directive beams (thus providing richer angular information than the 4 beams electronically switched in the BLE beacon of [28]).

To the authors knowledge, it is the first time that frequency-steering techniques are applied for angular estimation in a wireless personal area network (WPAN) paradigm with COTS devices such as BLE. A detailed comparison between different RSSI-based direction finding smart antenna

TABLE 6. Comparison between different RSSI-based DoD/DoA estimation techniques using smart antennas.

Ref.	Smart Antenna type	Frequency band	Steering Mechanism	DoA / DoD estimation algorithm	FoV	DoA / DoD mean error
[16]	Switched beam antenna (SBA)	2.45 GHz	Electronic switching between 4 radiation patterns, using a SP4T RF switch connected to four patch antennas	MUSIC	360º	20º
[20]	Electronically steerable parasitic array radiator (ESPAR) antenna.	2.45 GHz	Continuous electronic beam steering using seven electronically-controlled variable reactance RF diodes.	PPCC	360º	4º
[21]	Electronically steerable parasitic array radiator (ESPAR) antenna.	2.484 GHz	Discrete electronic beam steering using twelve RF switches.	PPCC	360º	8º
[22], [23]	Electronic steering dynamic monopulse receiver (DMR)	2.3 GHz / 2.45 GHz	Continuous electronic beam steering using two controllable RF phase-shifters and one hybrid coupler connected to two printed antennas.	monopulse technique	90º	3º
[25], [26]	Fixed monopulse.	868 MHz / 2.45 GHz	No beam steering, reduced field of view without ambiguities	monopulse technique	80º / 50º	6º / 3º
[27], [28]	Switched steering monopulse	2.480 GHz (BLE)	Electronic switching between 4 monopulse radiation patterns for BLE DoD, using a SP4T RF switch connected to a monopulse beam forming network (MBFN) and three patch antennas.	MUSIC	80º	9º
[29], [33], [34]	Electronically-steered leaky-wave antenna (ES-LWA)	2.45 GHz	Active antenna with two rows of RF varactor diodes controlled by two control signals.	MUSIC	80º / 120º	10º / 13º
[31]	Frequency-steered leaky-wave antenna (FS-LWA)	[2-3.5] GHz wide band	Passive antenna with frequency steering using wideband RF signal.	PPCC	180º	3º
[35]	Frequency-steered leaky-wave antenna (FS-LWA)	2.39GHz 2.52 GHz 2.65 GHz	Passive antenna with analog frequency-steered monopulse patterns using three RF channels.	monopulse technique	160º	2º
This work	Frequency-steered monopulse LWA array.	2.402 GHz 2.426 GHz 2.480 GHz	Passive antenna with digital BLE frequency-steered monopulse patterns using three RF channels.	monopulse technique	120°	3.7º

systems, including DoA and DoD, applied to IoT scenarios is done in next Section IV.

IV. COMPARISON WITH PREVIOUS SMART ANTENNA SYSTEMS FOR RSSI-BASED DIRECTION ESTIMATION

Table 6 summarizes the main smart antenna designs that have been proposed for power-based direction finding in the 2.45 GHz band. A Switched Beam Antenna (SBA) was used in [16] for DoA estimation for 2.4 GHz Zigbee WSN. It needs a Single Pole 4 through (SP4T) RF switch and control circuitry to switch between four patch antennas, which cover a total FoV of 360°. Due to the wide HPBW = 60° of each individual patch antenna, the adapted MUSIC algorithm leads to a high angular error of 20°. A more complex electronically steerable parasitic array radiator (ESPAR) antenna, formed by seven parasitic dipoles loaded with electronically-controlled variable-reactance RF diodes, was proposed in [20] for DoA estimation at 2.45 GHz. A high angular precision of 4° is obtained at the cost of the use of complex electronic beam steering control circuitry, which must tune seven control signals to perform the continuous beam steering. The ESPAR design proposed in [21] for WSN DoA estimation is composed by a higher number of 12 parasitic monopoles, thus increasing to this number the amount of control signals. However, they used RF switching instead of continuous controllable RF reactances, thus leading to simpler binary

control at the expense of losing pattern reconfiguration flexibility. As a consequence, lower angular resolution of 8° was obtained, but with simpler control hardware and associated signal processing. In [20] and [21], the power pattern cross-correlation (PPCC) method was used for DoA estimation. The use of monopulse techniques simplifies the reconfiguration circuitry while keeping high angular resolution, as it was demonstrated in [22] using an electronically steered dynamic monopulse receiver (DMR) for RSSI-DoA estimation operating at 2.3 GHz. In this case, the electronic steering circuitry makes use of two controllable phase-shifters and a 90° RF hybrid coupler, which are connected to two patch antennas. Now, only two control signals are needed by the Micro-Controller Unit (MCU) to reconfigure the RF phase shifters and produce a beam steering of the monopulse patterns in a FoV of 90°, obtaining 3° angular resolution.

Similarly, two printed dipole antennas were connected to a 180° RF hybrid coupler and two phase-shifters controlled by a MCU to perform 2.45 GHz RFID localization in [23], reporting similar 90° FoV and 4° angular discrimination. In [24]–[26], the use of static (not steered) monopulse patterns was proposed for direction finding, and thus the FoV without ambiguity and the angular accuracy is much reduced. In [25], an 868 MHz RFID RSSI-based monopulse reader for DoA estimation is designed for a wide FoV of 80°, obtaining a mean angular error of 6°. In [26], more directive antennas are used for 2.45 GHz WiFi RSSI-based monopulse sniffer, thus reporting narrower 50° FoV and lower mean angular error of 4°. Certainly, one needs very directive beams to increase the angular resolution, but this leads to reduced FoV unless the beams are somehow steered in space. In [27], an advanced BLE beam-switching monopulse beacon for only-RSSI DoD estimation is designed by connecting three patch antennas to a monopulse beam forming network (MBFN), comprised of three RF power combiners and two 90° hybrids, which are connected to a single BLE beacons using an RF SP4T switch. This complex active MBFN circuit synthesizes four radiation patterns, which ultimately creates two shifted monopulse patterns to eliminate ambiguities. The reported FoV and mean angular estimation error in [27] using an adapted version of MUSIC were, respectively, 80° and 9°. A last type of smart antenna used for RSSI-based DoA estimation is the electronically steered leaky-wave antenna (ES-LWA). In [29], a ES-LWA operating at a fixed frequency of 2.445 GHz was proposed for DoA estimation in a wide FoV of 80°, reporting an angular error of 10°. This ES-LWA needs two rows of 14 varactor diodes (28 in total), each row being controlled by two voltage signals and a MCU. Similarly, in [33], [34], a ES-LWA with 12+12 electronically controlled varactors was applied for DoA estimation, showing similar electronic steering in a wide 120° FoV, and reporting angular accuracy below 5° when using power-based adapted MUSIC algorithms [34].

Clearly in all the cases where electronic beam steering is present for wide FoV angular estimation with high resolution, there is a need of a MCU and active RF reconfiguration circuitry to perform the beam steering, thus increasing the overall costs and energy consumption if compared to a completely passive system. In this sense, frequency-steering leaky-wave antennas (FS-LWA) can synthesize several narrow beams covering a wide FoV by using frequency-modulated RF signals (non-fixed frequency), and this can be applied to direction finding as proposed in [30]–[32], [35]. More particularly, a wideband pulsed RF signal covering the 2 GHz – 3.5 GHz band, was applied in [31] to DoA estimation reporting very low angular estimation error of 3° in a wide FoV of 180°, and using a PPCC method. On the contrary, in [35] it was proposed the use of monopulse direction finding techniques with a multi-tone RF beacon signal composed of three narrowband tones at 2.39GHz, 2.52 GHz and 2.65 GHz (260 MHz total bandwidth), showing 2° mean error in a FoV of 160°.

In this work we have applied this multi-tone analog amplitude-monopulse DoA estimation proposal of [35] for *digital* BLE DoD estimation. As it was explained in Section II, the LWA array was adapted to use the three BLE advertising channels (2.402 GHz 2.426 GHz, and 2.480 GHz). The LWA array proposed in [35] had to be redesigned to meet this much narrower band of 78 MHz, while keeping a wide FoV. Moreover, another difference is that the processing is done in the digital domain and not in the analog RF domain. This means that the RSSI of the different channels can be first acquired and recorded, and later processed by combining RSSI from different frequencies, leading to *virtual* monopulse synthesis. For instance, a virtual monopulse pattern could be created combining the RSSI acquired at channel #37 with the RSSI of channel #39, as it was explained in Section II. This was not possible in the analog RF domain, where the powers received at different ports of the LWA array should be compared for the same frequency, as done in *simultaneous* monopulse technique. Finally, quantization errors due to BLE RSSI discretization in 1 dBm steps have reduced the angular resolution with respect to the analog version [35] from 2° to 3.7°. In any case, it has been demonstrated that the frequency-steered monopulse angular finding concept can be translated from the analog RF domain to the digital domain using COTS BLE hardware, which can lead to commercial application.

If compared to previous RSSI-based DoA/DoD estimation based on electronic-steering techniques, the frequency-steering technique dispenses from any active switching/phase-shifting RF beamforming network and associated MCU hardware, thus reducing the cost and power consumption. This is of key importance for cost-effective widespread applications, such as BLE in the context of the IoT and Smart Cities paradigm. Certainly, the BLE-beacon standard perfectly suits with this frequency-steering property of LWAs, since its advertising protocol produces the requested channel-hopping schedule without any modification in the BLE hardware or software. For the author's knowledge, it is the first time that a LWA array frequency-dispersion response

is designed to match the BLE standard for accurate and low-cost DoD estimation applications with this simplicity.

The main contribution of this paper is the use of the frequency steering technique to steer the directive beam and obtain the angular information for the DoD estimation. Once the steering data has been obtained, different DoA/DoD estimation algorithms such as MUSIC, PPCC or monopulse processing can be applied, as summarized in Table 6.

V. CONCLUSION

A novel system for RSSI-based DoD estimation using BLE bacons has been presented. Taking advantage of the inherent BLE channel-hopping advertising scheduling protocol, we have proposed for the first time the use of a frequency-beam-steering LWA array to create twelve partially-overlapped directive beams covering a wide FoV of 120°. This can create up to 13 monopulse functions steered in this wide FoV while keeping high angular sensitivity. In contrast to previous smart antenna designs, the proposed antenna array is extremely simple and low cost, since it is composed of a totally passive structure fabricated in low-cost PCB FR4 laminate, thus dispersing for RF switches, tunable RF components or any other type of active beam forming network and microcontroller unit to perform the electronic beam steering/switching. The LWA array has been designed to match the three advertising channels that are sequentially broadcasted by commercial BLE beacons, and centered at 2402 MHz (#37), 2426 MHz (#38), and 2480 MHz (#39).

The relative RSS levels produced by each one of the twelve synthesized beams are measured by the mobile device with BLE module, which sends this information to the software that estimates the DoD using simple amplitude-monopulse techniques. We have proposed a frequency steered monopulse function to construct a pseudospectrum that provides the DoD in the wide FoV covered by the array. Moreover, angular windowing can be applied to mitigate the effects of multipath and keep high angular estimation in the presence of unwanted reflections. Our system has shown a low root mean squared angular error of 3.7° in the wide 120° FoV, while keeping a totally passive smart antenna design. Also, the signal processing is extremely simple and with low computational load, since it involves simple comparison between acquired RSSI levels. This is of key importance in the context of the IoT and Smart Cities, where the use of the commercially-off-the-shelf (COTS) devices, low-cost antennas and low-power processing is preferable. In future works, these advanced low-cost BLE beacons will be used for indoor positioning.

REFERENCES

[1] K. E. Jeon, J. She, P. Soonsawad, and P. C. Ng, "BLE beacons for Internet of Things applications: Survey, challenges, and opportunities," *IEEE Internet Things J.*, vol. 5, no. 2, pp. 811–828, Apr. 2018.

[2] S. Alletto, R. Cucchiara, G. Del Fiore, L. Mainetti, V. Mighali, L. Patrono, and G. Serra, "An indoor location-aware system for an IoT-based smart museum," *IEEE Internet Things J.*, vol. 3, no. 2, pp. 244–253, Apr. 2016.

[3] M. S. Gast, *Building Applications with IBeacon: Proximity and Location Services with Bluetooth Low Energy*. Sebastopol, CA, USA: O'Reilly Media, 2014.

[4] *Specification of the Bluetooth System. Core Version 4.0*, Bluetooth, Kirkland, WA, USA, Jun. 2010.

[5] *Specification of the Bluetooth System. Core Version 5.1*, Bluetooth, Kirkland, WA, USA, Jan. 2019.

[6] P. Spachos, I. Papapanagiotou, and K. N. Plataniotis, "Microlocation for smart buildings in the era of the Internet of Things: A survey of technologies, techniques, and approaches," *IEEE Signal Process. Mag.*, vol. 35, no. 5, pp. 140–152, Sep. 2018.

[7] Y. Gu and F. Ren, "Energy-efficient indoor localization of smart hand-held devices using Bluetooth," *IEEE Access*, vol. 3, pp. 1450–1461, 2015.

[8] S. Sadowski and P. Spachos, "RSSI-based indoor localization with the Internet of Things," *IEEE Access*, vol. 6, pp. 30149–30161, 2018.

[9] L. Chen, L. Pei, H. Kuusniemi, Y. Chen, T. Kröger, and R. Chen, "Bayesian fusion for indoor positioning using Bluetooth fingerprints," *Wireless Pers. Commun.*, vol. 70, no. 4, pp. 1735–1745, Jun. 2013.

[10] R. Faragher and R. Harle, "Location fingerprinting with Bluetooth low energy beacons," *IEEE J. Sel. Areas Commun.*, vol. 33, no. 11, pp. 2418–2428, Nov. 2015.

[11] K. Kalliola. (2011). High accuracy indoor positioning based on BLE. Nokia Research Center Presentation, Espoo, Finland. Accessed: Jan. 1, 2020. [Online]. Available: https://docplayer.net/43792139-High-accuracy-indoor-positioning-based-on-ble.html

[12] N. Honma, R. Tazawa, K. Kikuchi, A. Miura, Y. Sugawara, and H. Minamizawa, "Indoor-positioning using RSSI?: DOD-based technique versus RSSI-ranging technique," in *Proc. 8th Int. Conf. Indoor Positioning Indoor Navig. IPI*, 2017, Art. no. WIP171.

[13] L. Godara, "Application of antenna arrays to mobile communications. II. Beam-forming and direction-of-arrival considerations," *Proc. IEEE*, vol. 85, no. 8, pp. 1195–1245, Aug. 1997.

[14] J. Gjengset, J. Xiong, G. Mcphillips, and K. Jamieson, "Phaser: Enabling phased array signal processing on commodity WiFi access points," in *Proc. 20th Annu. Int. Conf. Mobile Comput. Netw.-(MobiCom)*, 2014, pp. 153–164.

[15] S. Monfared, T.-H. Nguyen, L. Petrillo, P. De Doncker, and F. Horlin, "Experimental demonstration of BLE transmitter positioning based on AOA estimation," in *Proc. IEEE 29th Annu. Int. Symp. Pers., Indoor Mobile Radio Commun. (PIMRC)*, Sep. 2018, pp. 856–859.

[16] S. Maddio, A. Cidronali, and G. Manes, "RSSI/DoA based positioning systems for wireless sensor network," in *New Approach Indoor Outdoor Localization System*. Rijeka, Croatia: InTech, 2012, ch. 7, pp. 139–162.

[17] L. Brás, N. B. Carvalho, P. Pinho, L. Kulas, and K. Nyka, "A review of antennas for indoor positioning systems," *Int. J. Antennas Propag.*, vol. 2012, pp. 1–14, Oct. 2012.

[18] G. Giorgetti, S. Maddio, A. Cidronali, S. K. S. Gupta, and G. Manes, "Switched Beam Antenna Design Principles for Angle of Arrival Estimation," in *Proc. Eur. Wireless Technol. Conf.*, Sep. 2009, pp. 5–8.

[19] C. Sun and N. C. Karmakar, "Direction of arrival estimation with a novel single-port smart antenna," *EURASIP J. Appl. Signal Process.*, vol. 2004, no. 9, 2004, Art. no. 484138.

[20] E. Taillefer, A. Hirata, and T. Ohira, "Direction-of-arrival estimation using radiation power pattern with an ESPAR antenna," *IEEE Trans. Antennas Propag.*, vol. 53, no. 2, pp. 678–684, Feb. 2005.

[21] L. Kulas, "RSS-based DoA estimation using ESPAR antennas and interpolated radiation patterns," *IEEE Antennas Wireless Propag. Lett.*, vol. 17, no. 1, pp. 25–28, Jan. 2018.

[22] J.-C. Wu, C.-C. Chang, T.-Y. Chin, S.-F. Chang, M.-C. Chiu, C.-Y. Hsu, and R.-H. Lee, "Wireless indoor localization using dynamic monopulse receiver," in *Proc. 7th Eur. Radar Conf.*, Sep./Oct. 2010, pp. 69–72.

[23] M. Del Prete, D. Masotti, N. Arbizzani, and A. Costanzo, "Remotely identify and detect by a compact reader with mono-pulse scanning capabilities," *IEEE Trans. Microw. Theory Techn.*, vol. 61, no. 1, pp. 641–650, Jan. 2013.

[24] M. Hartmann, O. Pfadenhauer, L. Patino-Studencka, H.-M. Tröger, A. Heuberger, and J. Thielecke, "Antenna pattern optimization for a rssi-based direction-of-arrival localization system," in *Proc. ION's Pacific PNT Conf.*, Mar. 2015, pp. 429–433.

[25] Y. Á. López, M. E. De Cos Gómez, and F. Las-Heras Andrés, "A received signal strength RFID-based indoor location system," *Sens. Actuators A, Phys.*, vol. 255, pp. 118–133, Mar. 2017.

[26] J. L. Gomez-Tornero, D. Canete-Rebenaque, J. A. Lopez-Pastor, and A. S. Martinez-Sala, "Hybrid analog-digital processing system for amplitude-monopulse RSSI-based MiMo WiFi direction-of-arrival estimation," *IEEE J. Sel. Topics Signal Process.*, vol. 12, no. 3, pp. 529–540, Jun. 2018.

[27] N. Honma, R. Tazawa, A. Miura, Y. Sugawara, and H. Minamizawa, "RSS-based DOA/DOD estimation using Bluetooth signal and its application for indoor tracking," in *Proc. Int. Conf. Indoor Positioning Indoor Navigat. (IPIN)*, Sep. 2018, pp. 1–7.
[28] R. Tazawa, N. Honma, A. Miura, and H. Minamizawa, "RSSI-based localization using wireless beacon with three-element array," *IEICE Trans. Commun.*, vol. E101.B, no. 2, pp. 400–408, 2018.
[29] S. Abielmona, H. V. Nguyen, and C. Caloz, "Analog direction of arrival estimation using an electronically-scanned CRLH leaky-wave antenna," *IEEE Trans. Antennas Propag.*, vol. 59, no. 4, pp. 1408–1412, Apr. 2011.
[30] A. J. Martinez-Ros, J. L. Gomez-Tornero, and G. Goussetisy, "Frequency scanning leaky wave antenna for positioning and identification of RFID tags," in *Proc. IEEE Int. Conf. RFID-Technol. Appl.*, Sep. 2011, pp. 451–456.
[31] X. Yu and H. Xin, "Direction of arrival estimation utilizing incident angle dependent spectra," in *IEEE MTT-S Int. Microw. Symp. Dig.*, Jun. 2012, pp. 1–3.
[32] Q. Liu, V. Fusco, D. Linton, and D. Zelenchuk, "Frequency scanning antenna for target location applications," in *Proc. 8th Eur. Conf. Antennas Propag. (EuCAP)*, Apr. 2014, pp. 2059–2061.
[33] J. Werner, J. Wang, A. Hakkarainen, N. Gulati, D. Patron, D. Pfeil, K. Dandekar, D. Cabric, and M. Valkama, "Sectorized antenna-based DoA estimation and localization: Advanced algorithms and measurements," *IEEE J. Sel. Areas Commun.*, vol. 33, no. 11, pp. 2272–2286, Nov. 2015.
[34] H. Paaso, N. Gulati, D. Patron, A. Hakkarainen, J. Werner, K. R. Dandekar, M. Valkama, and A. Mammela, "DoA estimation using compact CRLH leaky-wave antennas: Novel algorithms and measured performance," *IEEE Trans. Antennas Propag.*, vol. 65, no. 9, pp. 4836–4849, Sep. 2017.
[35] M. Poveda-Garcia, D. Canete-Rebenaque, and J. L. Gomez-Tornero, "Frequency-scanned monopulse pattern synthesis using leaky-wave antennas for enhanced power-based direction-of-arrival estimation," *IEEE Trans. Antennas Propag.*, vol. 67, no. 11, pp. 7071–7086, Nov. 2019.
[36] S. Ishida, Y. Takashima, S. Tagashira, and A. Fukuda, "Design and initial evaluation of Bluetooth low energy separate channel fingerprinting," in *New Trends in E-service and Smart Computing*, vol. 742. Cham, Switzerland: Springer, 2018, pp. 19–33.
[37] *BlueZ Library-Linux Bluetooth Protocol Stack*. Accessed: Dec. 9, 2019. [Online]. Available: http://www.bluez.org/
[38] *Parani-UD100 Bluetooth 4.0 Class1 USB Adapter*. Accessed: Feb. 18, 2019. [Online]. Available: http://www.senanetworks.com/ud100-g03.html?sc=14&category=3968
[39] G. Zelinski, G. Thiele, M. Hastriter, M. Havrilla, and A. Terzuoli, "Half width leaky wave antennas," *IET Microw. Antennas Propag.*, vol. 1, no. 2, p. 341, 2007.
[40] M. Poveda-García, J. L. Gómez-Tornero, and D. Cañete-Rebenaque, "Study of the efficiency of half-width substrate integrated waveguide leaky-wave antennas in FR4," in *Proc. 2nd URSI Atlantic Radio Sci. Meeting (AT-RASC)*, May/Jun. 2018, pp. 1–4.
[41] A. A. Oliner and D. R. Jackson, "Leaky-wave antennas," in *Antenna Engineering Handbook*, J. L. Volakis, Ed., 4th ed. New York, NY, USA: McGraw-Hill, 2007.
[42] R. Schmidt, "Multiple emitter location and signal parameter estimation," *IEEE Trans. Antennas Propag.*, vol. AP-34, no. 3, pp. 276–280, Mar. 1986.
[43] R. Roy and T. Kailath, "ESPRIT-estimation of signal parameters via rotational invariance techniques," *IEEE Trans. Acoust., Speech, Signal Process.*, vol. 37, no. 7, pp. 984–995, Jul. 1989.
[44] M. A. Tehrani, Y. Savaria, and J. J. Laurin, "Multiple targets direction-of-arrival estimation in frequency scanning array antennas," *IET Radar, Sonar Navigat.*, vol. 10, no. 3, pp. 624–631, Mar. 2016.
[45] A. Cardama-Aznar, L. Jofre-Roca, J. M. Rius-Casals, J. Romeu-Robert, and S. Blanch-Boris, *Antenas*. Barcelona, Spain: El Tinter, 2002.

MIGUEL POVEDA-GARCÍA was born in Pozohondo, Spain, in 1992. He received the degree in telecommunications engineering and the master's degree in telecommunications engineering from the Technical University of Cartagena, Cartagena, Spain, in 2014 and 2016, respectively, where he is currently pursuing the Ph.D. degree. His Ph.D. is focused on the analysis of the dispersion of planar leaky-wave antennas in substrate integrated waveguide technology and their design for different applications. His research interests include leaky-wave antennas and their application in telecommunication systems, the Internet of Things, and energy harvesting.

ANTONIO GÓMEZ-ALCARAZ was born in San Javier, Spain, in 1994. He received the degree in telecommunications engineering from the Technical University of Cartagena, Spain, in 2017, where he is currently pursuing the master's degree in telecommunications engineering. His research interests include leaky-wave antennas and their application in telecommunication systems, indoor location systems, and the IoT.

DAVID CAÑETE-REBENAQUE was born in Valencia, Spain, in 1976. He received the telecommunications engineering degree from the Technical University of Valencia, Valencia, in 2000, and the Ph.D. degree from the Technical University of Cartagena, Cartagena, Spain, in 2009. In 2001, he joined the Mobile Communication Company, as an RF Engineer. In 2002, he joined the Communications and Information Technologies Department, Technical University of Cartagena, where he is involved in research and teaching activities. His current research interest includes the analysis and design of microwave circuits and antennas.

ALEJANDRO SANTOS MARTINEZ-SALA was born in Cehegin, Spain, in 1976. He received the degree in electrical engineering, in 2000, and the Ph.D. degree in telecommunications from the Universidad Politécnica de Cartagena (UPCT), Spain, in 2006. In 2001, he joined UPCT, where he is currently an Assistant Professor with the Communications and Information Technologies Department. His research interests include the indoor and outdoor location systems with the IoT, innovation management, and technology transfer to industry.

JOSÉ LUIS GÓMEZ-TORNERO (Senior Member, IEEE) was born in Murcia, Spain, in 1977. He received the degree in telecommunications engineering from the Technical University of Valencia, Valencia, Spain, in 2001, and the Ph.D. degree from the Technical University of Cartagena (UPCT), Cartagena, Spain, in 2005. In 2000, he joined the Radio Frequency Division, Industry Alcatel Espacio, Madrid, Spain. In 2001, he joined UPCT, where he has been an Associate Professor, since 2008, and a Full Professor, since 2019. He was the Vice Dean for Students and Lecturers affairs as a member of the Telecommunication Engineering Faculty. He has been a Visiting Researcher/Professor with the University of Loughborough, U.K., Heriot-Watt University, Edinburgh, U.K., Queen's University of Belfast, U.K., and CSIRO-ICT Centre, Sydney, NSW, Australia. In February 2010, he was appointed as a CSIRO Distinguished Visiting Scientist by the CSIRO ICT Centre. He has coauthored more than 80 peer-reviewed journal articles, and more than 150 conference papers. His current research interests include the analysis and design of leaky-wave devices and their applications, and the innovation in the area of higher education. His research work has received various awards, including the EPSON-Ibérica Foundation (2004) and Vodafone Foundation (2005) awards to the Best Ph.D. Thesis in the area of advanced mobile communications technologies, Hispasat (2014) and Hisdesat (2015) prizes to the Best Ph.D. Thesis in satellite communication technologies. Also, he was a co-recipient of the 2010 IEEE Engineering Education Conference Award, the 2011 EuCAP Best Student Paper Prize, the 2012 EuCAP Best Antenna Theory Paper Prize, the 2012 and 2013 Spanish URSI Prize for the Best Student Paper, the 2013 APS Best Student Paper finalist, and the 2018 iWAT Best Poster Award.